Stress transfer characteristics of sheathed strand in prestressed concrete beams: computational study

Rigoberto Burgueño and Yi Sun

- Damage during manufacture of pretensioned beams with debonded strands has raised concerns about the use of debonding as currently specified.
- Nonlinear finite element models of small-scale prestressed concrete beams were analyzed to improve understanding of the stress transfer characteristics of sheathed strand in pretensioned concrete elements and calibrated with experimental data.
- The results show that the lack of bond resistance along the debonded region maximizes the dilation of the strand after release, leading to damage of the concrete if there is tight contact between concrete and strand.

The debonding of strands is an accepted method to reduce the stresses at the ends of prestressed concrete beams,[1,2] yet damage in the anchorage zones of beams with debonded strands during the production of box beams[3,4] (**Fig. 1**) and U beams[5] for bridges in Michigan and Indiana, respectively, has brought into question the bond behavior of sheathed strands. While strand bond has been extensively studied, many aspects associated with this important design feature, particularly when dealing with sheathed strand, are still based on limited experimental evidence, and design and production practices rely heavily on empirical knowledge.

Debonding is typically achieved by placing plastic sheathing around the strand to reduce or eliminate the bond with concrete. Two sheathing options are commonly used: flexible slit sheathing with a tight fit around the strand or a more rigid closed tube with an inside diameter larger than the strand. Flexible (softer) debonding material can deform under hydraulic pressure after concrete is placed and thus form a tight fit around the strand. Such tight fitting is thought to lead to lower debonding efficiency due to residual mechanical interlock or the infiltration of cement paste (or slurry) through the slit in the sheathing. By contrast, use of an oversized preformed closed tube physically separates the strand from the concrete, thus eliminating all bond.

Figure 1. End damage observed on skewed bridge box beams during production.

Several experimental and computational studies have evaluated the efficiency of strand debonding in reducing beam-end stresses,[6–10] yet the focus has largely been on longitudinal stress transfer behavior. However, an effect that has received less attention related to strand debonding is the lateral behavior, or dilation, of the strand. As is well known, a strand will expand radially due to Poisson's effect once it is released. This expansion is thought to be a possible reason for beam-end cracking in prestressed concrete girders with partially debonded, or shielded, strand.[9] Direct experimental measurements of this mechanism are difficult, if not impossible. As a result, it is necessary to use computational simulations to evaluate strand bond behavior using three-dimensional (3-D) strand models.

The stress transfer mechanism between strand and concrete in pretensioned concrete products is attributed to adhesion, mechanical interlock, and friction,[11] depending on the stage of bond development and the nature of the strand surface. While the strand-concrete bond mechanisms have been investigated from multiple points of view, the complicated stress state at the end of pretensioned concrete products upon stress transfer continues to be a topic of research significance given that unanticipated problems with beam-end cracking persist. Several studies have been conducted to address the beam-end cracking problem in pretensioned concrete beams, in which experimental studies have often been combined with analytical and numerical approaches to provide a better understanding. Mirza and Tawfik[6] conducted an experimental study combined with a relatively simple analytical model to understand the appearance of vertical cracks in the end region of pretensioned members during detensioning. Although the study provided several useful findings, the model developed by Mirza and Tawfik was one-dimensional and based on the assumption of linear-elastic behavior for concrete and steel, a frictionless casting bed, and negligible dynamic effects. Furthermore, the use of linear beam theory could not reflect the 3-D character of the stress state in the beam-end region.

A further study of the end cracking of pretensioned I-shaped concrete girders was performed by Kannel et al.[8] Three-dimensional elastic finite element analyses were conducted to assess the stress state at the girder end upon detensioning. The anchorage region was modeled with solid continuum elements, and beam elements were used for the remainder of the girder. The pretensioning strands were simulated with truss elements. The researchers noted that although the models used linear elastic materials, their goal was not to determine stresses exactly, but rather to identify trends in the stress fields. The study conducted by Kannel et al. provided useful findings, yet because they used truss elements to model the strands, they were not able to incorporate the expansion of the strand after release and thus capture a realistic stress state in the anchorage zone.

Okumus and Oliva[10] conducted nonlinear finite element analyses to evaluate methods for crack control at the ends of prestressed bridge girders. Bulb-tee girders were modeled with 3-D solid elements to assess global damage, but the strands themselves, not being part of the study focus, were excluded from the model. Their effect was instead modeled by applying linearly increasing surface stresses along the strand transfer length, which was taken as 60 times the strand diameter.

Definition of the interaction between strand and concrete when conducting finite element simulations defines the type of behavior that can be captured and is, thus, critical. Kannel et al. modeled such interaction by using nonlinear springs, which require the definition of one-to-one node pairs and are only useful when the strands are simplified by truss or beam elements, for which the number of node pairs is limited. If solid, or brick, elements are used for both strand and concrete, the large amount of nodes generated along the interacting surfaces makes it impractical to define spring elements with node-to-node bond characteristics. Other modeling approaches used by researchers include assuming a perfect bond or a friction contact[12] response between the strand and the surrounding concrete. However, assuming perfect bond will lead to unrealistic, high stresses in the end region of the concrete beam and misrepresent any findings on the stress state in the anchorage region because the bond-slip behavior cannot be captured.

This paper presents a computational study aimed at investigating the 3-D stress transfer behavior of sheathed strand in prestressed concrete beams. Nonlinear finite element analyses were conducted using commercial software. The strand was simulated with 3-D continuum solid elements, and its interaction with concrete in bonded and debonded regions was simulated using surface-based contact interaction definitions. The effects of debonding method (tight-fitting flexible sheathing and oversized rigid tubing), debonded length, and strand spacing were evaluated. The numerical models were calibrated with data from a companion experimental study.[4,13]

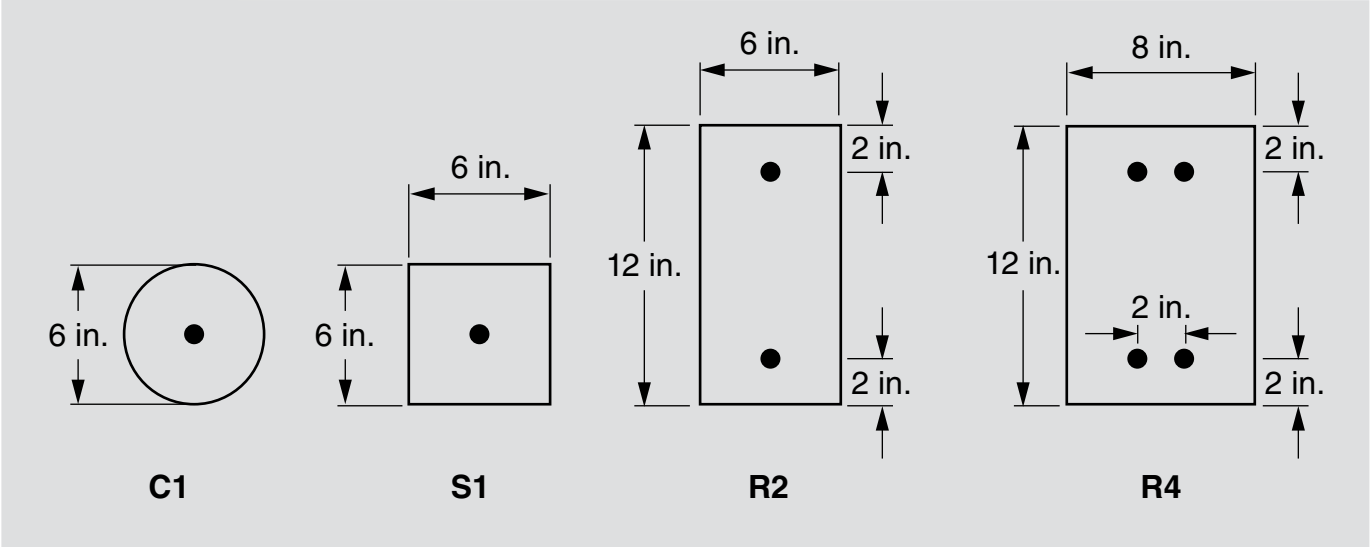

Figure 2. Cross sections of prestressing beam units modeled. The dark circles represent the 0.6 in. diameter strand. Note: 1 in. = 25.4 mm.

The stress transfer mechanisms from a twisted seven-wire strand onto a concrete element along with the multiple influencing parameters exceed in complexity what can be accomplished even with the enhanced simulation approach attempted in this work. Thus, the approach and findings in this study are not to be evaluated for their exact predictive ability but rather for the insight that they provide in terms of behavior, for which they are considered to be reliable.

Model geometries

As noted, this numerical study complements an experimental investigation on the stress transfer characteristics of sheathed strand in which 24 small-scale beams were tested.[4,13] The test beams were divided into four groups (of six units each) based on their cross sections and the number of strands (**Fig. 2**). The experimental program investigated the influence of release method (sudden release versus gradual release), debonded material (flexible/soft slit sheathing versus rigid, oversized, preformed tubing), and debonded length on stress transfer. Each beam was named using the beam group name and the parameters investigated (**Fig. 3**). The numerical models were given the same identifying name as the corresponding beams in the experiments. The dynamic effect of sudden strand release was not modeled. Thus, the simulations focused on assessing the effect of debonding material, debonded length, and adjacent strands.

Finite element models were established and calibrated for the 24 beams in the experimental study.[13] However, this paper focuses on the results from eleven beams with circular (C1) and rectangular (R2 and R4) cross sections (Fig. 2) because the strands in these beams were released in the same manner, and the results from the square (S1) beams were similar to the C1 beams. **Table 1** gives geometrical and material details for the selected experimental beam units. The C1 beams were used to investigate the radial dilation effect of a single strand in fully bonded and partially debonded prestressed concrete beams. Beams with multiple strands (R2 and R4) were used to study the effect of debonded length and the interaction between adjacent strands. In all cases, only half of the beam length was modeled due to symmetry about the midsection, and appropriate symmetry boundary conditions were defined. In addition, the centroid of the section in the symmetry plane was fixed to eliminate rigid body motions. The casting bed was not modeled and no vertical constraints were applied to the bottom surface of the beam models because the vertical deformation is minimal due to the concentrically distributed strands. **Figure 4** shows views of the finite element models for the different beam cross sections.

Material constitutive models

Inelastic material behavior was used for the concrete model parts to capture the potential damage to the concrete during release of the pretensioned strand. The concrete damage plasticity model[14] in the commercial software was used. The model by Collins[15] was used to define the backbone envelope for concrete compressive and tensile behavior based on peak strengths from standard material tests.[4,13] The concrete modulus of elasticity was defined according to *Building Code Requirements for Structural Concrete (ACI 318-08) and Commentary (ACI 318R-08)*[16] using the experimental concrete compressive strength at the day of test (release) (Table 1). Poisson's ratio for concrete was assumed to be 0.2. **Table 2** shows the parameters used for the inelastic concrete material definition for beam C1.00.NG

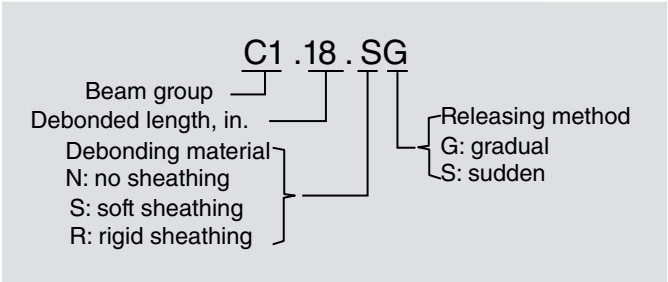

Figure 3. Naming convention used to identify different beam units.

Table 1. Experimental test matrix for stress transfer evaluation of pretensioned strand

Beam	L, ft	L_b, ft	L_u, ft	Debonded material	f'_{ci}, psi
C1.00.NG	20	20	0	n/a	5860
C1.00.NS	20	20	0	n/a	6050
C1.18.SS	20	17	1.5	Soft	6050
C1.18.RS	20	17	1.5	Rigid	6050
R2.00.NS	20	20	0	n/a	7153
R2.18.SS	20	17	1.5	Soft	7153
R2.36.SS	20	14	3	Soft	7153
R2.60.SS	20	10	5	Soft	7153
R4.00.NS	20	20	0	n/a	7371
R4.36.SS	20	14	3	Soft	5707
R4.60.SS	20	10	5	Soft	5707
R4.36.RS	20	14	3	Rigid	6857

Note: f'_{ci} = concrete compressive strength at day of test; L = beam length; L_b = bonded region length; L_u = unbonded region length; n/a = not applicable. 1 ft = 0.305 m.; 1 psi = 6.895 kPa.

as a representative example.

All beams in the experimental study[4,13] used 0.6 in. (15 mm) diameter seven-wire low-relaxation prestressing strand. Based on the manufacturer's material certification, the strand had an effective area of 0.2175 in.^{2} (140.3 mm^2), an elastic modulus of 29,000 ksi (200,000 MPa), and an ultimate strength of 270 ksi (1860 MPa). The prestressing strand remained within its proportionality limit during stressing and transfer. Thus, the 3-D strand model parts were assigned a linear elastic material. A Poisson's ratio of 0.3 was assumed for the strand.

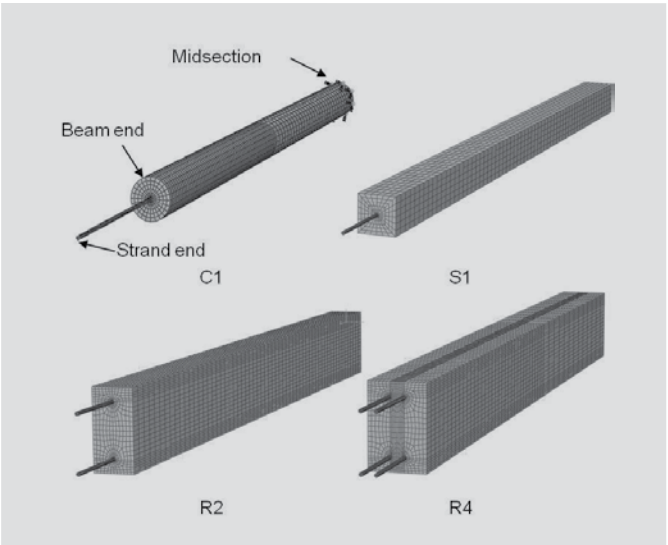

Figure 4. Finite element models for different beam cross sections.

Simulation of prestress and strand-concrete bond

Strand modeling

Due to the complex geometry of the bundle of seven twisted wires, the strand model was simplified to have a circular cross section of equivalent area. The computational demand was thus significantly reduced while the radial expansion of the strand due to Poisson's effect after release was still captured.

Strand pretensioning

Three-dimensional eight-node linear continuum (solid) elements with reduced integration were used for both the concrete and prestressing strand parts in the finite element models. The equivalent diameter of the solid strand in the models was calculated based on the net cross-sectional area of the strand. The pretensioned state in the strands was simulated by introducing an initial stress condition in the longitudinal direction, which means that the strand in the finite element model is already tensioned. As a result, the diameter of the modeled strands was further reduced to account for the pretensioning force. The final diameter for the strands used in the models was calculated to be 0.5245 in. (13.32 mm) for all strands. The magnitude of the initial stress in the strand (pretensioned force) was determined based on experimental data from the tensioning process (strand jacking force minus seating losses).[4,13]

Strand-concrete bond definition

Because the mechanical interlock component of bond

Table 2. Concrete material model parameters for C1.00.NG beam model

Strand properties	E_p, ksi		29,000	
	Poisson's ratio		0.3	
Concrete elastic properties	E_c, ksi		4363	
	Poisson's ratio		0.2	
Parameters for concrete damage plasticity model	Dilation angle		37	
	Eccentricity		0.1	
	$\sigma_{b0} / \sigma_{c0}$		1.16	
	K		0.667	
	Viscosity parameter		0.005	
Concrete inelastic behavior	Concrete compression hardening		Concrete tension stiffening	
	Stress, ksi	Crushing strain	Stress, ksi	Cracking strain
	2.17	0.00000	0.57	0
	3.20	0.00002	0.34	0.00085
	4.91	0.00013	0.24	0.00389
	5.83	0.00066	0.18	0.00992
	4.19	0.00179	n.d.	n.d.
	2.51	0.00292	n.d.	n.d.
	1.09	0.00450	n.d.	n.d.
	0.42	0.00640	n.d.	n.d.

Note: E_c = elastic modulus of concrete at day of test; E_p = elastic modulus of prestressing strand at day of test; K = ratio of the second stress invariant on the tensile meridian to that on the compressive meridian at initial yield for any given value of the pressure invariant such that the maximum principal stress is negative; n.d. = no data; $\sigma_{b0} / \sigma_{c0}$ = ratio of initial equibiaxial compressive yield stress to the initial uniaxial compressive yield stress. 1 ksi = 6.895 MPa.

resistance cannot be explicitly captured by modeling the strand as a smooth rod, the tangential surface interaction property defined between the circular strand and the surrounding concrete included the effects of adhesion and mechanical interlock. However, the Poisson's, or Hoyer, effect is automatically included in the simulation by virtue of modeling the strand as a 3-D deformable solid.

In the fully bonded region and in the debonded regions where soft tight-fitting sheathing material was used, the bond simulation was established by defining a surface-to-surface contact constraint. A hard contact surface interaction was defined between the strand surface and the surrounding concrete surface in the normal direction, which means that the two surfaces cannot penetrate each other and pressure can be generated at the interface. In the tangential direction a nonlinear friction model was defined between the two surfaces. The friction model is controlled by two parameters; namely, the contact pressure and a friction coefficient. When the prestressing strand is released, it will shorten longitudinally and dilate laterally due to Poisson's effect. Strand dilation is constrained by the surrounding concrete, generating pressure between the strand and the surrounding concrete. This pressure was used as the pressure necessary for the friction model. The friction coefficient, which controls the friction force per unit area for a given surface interaction pressure, was thus considered to be the parameter that controlled the bond resistance mechanism between strand and concrete in the simulation. In addition, bond slip was allowed to occur when the shear stress between strand and concrete exceeded a critical value, which was defined by the product of the contact pressure and the friction coefficient. As a result, the friction coefficient was an essential parameter for the bond simulation and its value was determined by calibrating the 3-D finite element models with the experimental data from prestressed concrete beams from the companion study.[4,13]

Debonded/blanketed strand

Two different debonding materials were considered in the simulations, namely, debonding by means of a tight-fitting

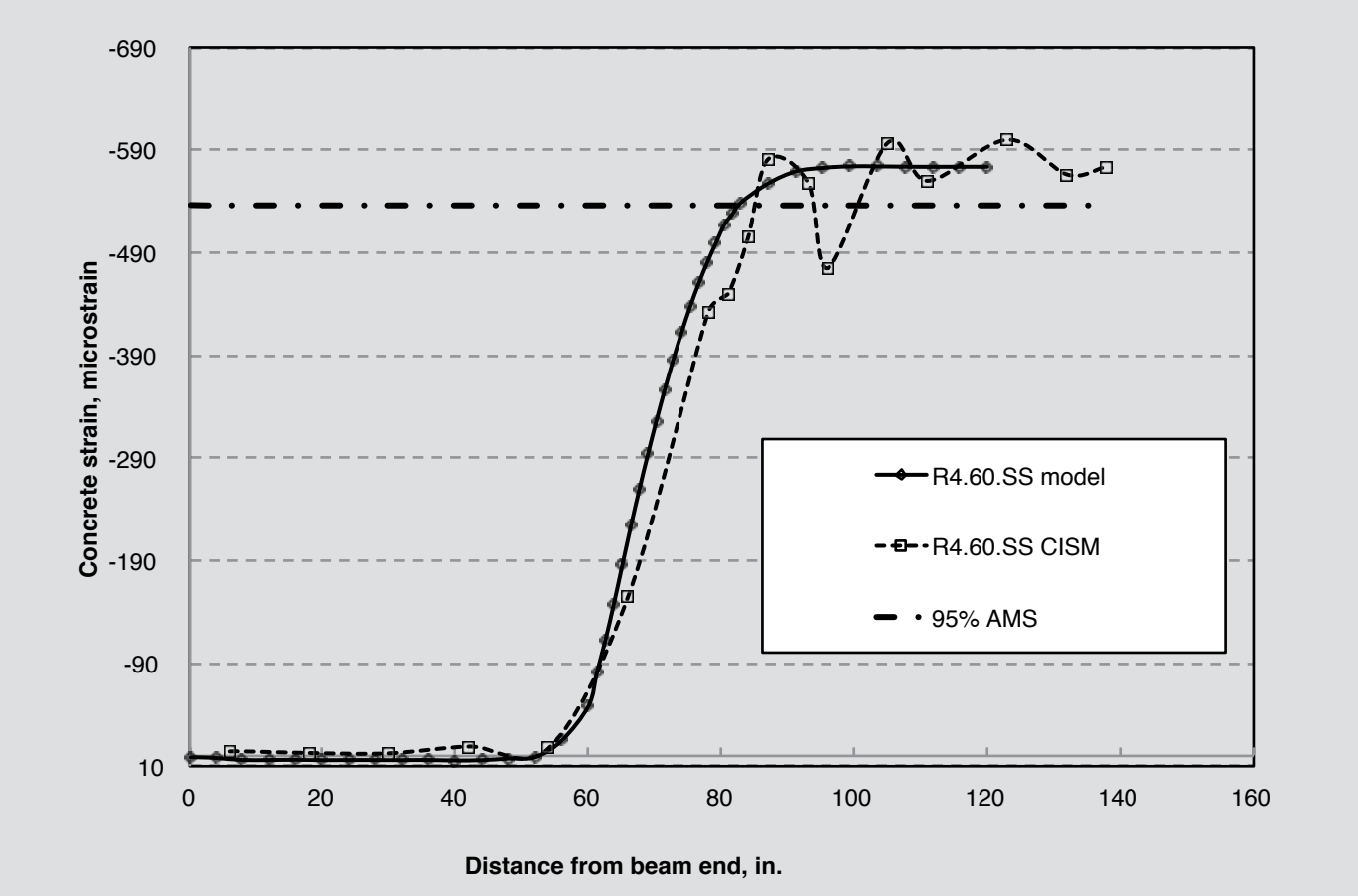

Figure 5. Calibration of finite element model for beam R4.60.SS based on experimental data from concrete internal strain measurements. Note: AMS = average maximum strain; SS = soft sheathing with sudden strand release. 1 in. = 25.4 mm.

flexible sheathing and debonding by means of an oversized rigid polymer tube.[4,13] The bond between strand and concrete is clearly zero when an oversized debonding tube is used because there is no physical contact between the strand and concrete. Thus, strand debonded with an oversized rigid sheathing material was simulated by defining oversized holes around the strand in the debonded region of the concrete part. The diameter of the oversized hole in the simulation was 0.6 in. (15 mm), which was considered to be oversized compared with the reduced diameter of the strand model (0.5245 in. [13.32 mm]). On the other hand, experimental results show that soft debonding material cannot eliminate the shear-slip resistance, or effective bonding strength, completely and that some force can be transferred along the debonded region. The mechanism behind this phenomenon is thought to be identified by the study reported in this paper and is discussed later. Nonetheless, the experimental program showed that transferred force along the debonded length was small compared with the total force in the strand. As a result, the bond strength, or the friction coefficient, between the strand and the surrounding concrete in the debonded strand region for all the beams using flexible, tight-fitting sheathing was set to zero. However, a tight fit was defined between the debonded strand and concrete by creating holes on the concrete part with the same diameter as the strand. A hard contact interaction was defined in the normal direction of the interacting surfaces along the debonded region so that pressure could be generated.

Model calibration

The finite element models were calibrated by adjusting the friction coefficient parameter in the surface interaction definition so as to match the concrete strain profiles from prestress transfer in the numerical models to the experimental data from Burgueño and Sun.[4,13] Concrete internal strains used for calibration were measured by strain gauges on a threaded rod that was embedded in the test beams. The instrumented rod was parallel to the strand and located 1 in. (25 mm) above the strand surface for the beams with one strand (C1 and S1) and at the centroid of the beam cross section for beams with multiple strands (R2 and R4). An important parameter in the concrete strain profile is the transfer length region. The 95% average maximum strain method[17] was adopted to determine transfer length, which was obtained as the distance from the point where the debonded region ends (or from the beam end for fully bonded beam units) to the point where the 95% average maximum strain line intersects the concrete strain profile (**Fig. 5**). Each model was calibrated with the experimental concrete strain profile for the corresponding beam unit.

Table 3. Calibrated friction coefficients of beam models

Beam	$L_{t,Exp}$, in.	$L_{t,FE}$, in.	μ_b
C1.00.NS	40.5	39.0	0.23
C1.18.SS	41.0	40.5	0.23
C1.18.RS	30.5	29.0	0.50
R4.00.NS	22.5	26.0	0.50
R4.36.SS	26.5	25.0	0.70
R4.60.SS	25.5	25.0	0.70
R4.36.RS	33.0	31.5	0.45

Note: $L_{t,Exp}$ = transfer length from experimental data; $L_{t,FE}$ = transfer length from finite element data; μ_b = friction coefficient between strand and concrete in finite element model along the bonded region. 1 in. = 25.4 mm.

Concrete creep and shrinkage strains were found to be significant in the small beam units due to delays in the measurement procedures during the experiment and thus had to be taken into account for proper use of the experimental data.[4,13] However, it was not possible to accurately simulate creep and shrinkage effects for each beam due to the lack of data on parameters such as temperature, relative humidity, and creep coefficients. Creep and shrinkage strains have the effect of shifting the effective strain in the beam but do not change the transfer length. In other words, the bond transfer behavior is not affected. Because the goal was to calibrate the coefficient of friction that simulates bond stress transfer, it was decided that it was unnecessary to precisely model concrete creep and shrinkage strains. Therefore, estimated concrete volume strains for each beam were added to the numerical models by introducing a temperature field on the concrete part. The magnitude of the temperature field was determined for each beam based on the required additional concrete strain.

Table 3 gives the calibrated friction coefficients between strand and concrete μ_b and the experimental and simulated transfer length values for the C1 and R4 beams. The table also provides the transfer length determined based on experimental data $L_{t,Exp}$ and simulated data $L_{t,FE}$. The differences in the coefficients determined for each beam model reflect the effects of concrete strength, debonding material, debonding length, and experimental variance. No reliable test data was available for the R2 beams due to instrumentation errors. Thus, the coefficient of friction used for these beam models (μ_b equal to 0.38) was the average value for the calibrated coefficients of all beams that were equally released after normalization for the different concrete compressive strengths.[4,13]

Simulation results

The stress transfer characteristics of bonded and debonded strand were studied using the results from the established numerical models. Concrete damage was studied primarily based on contour plots and traces of maximum principal stresses and strains.

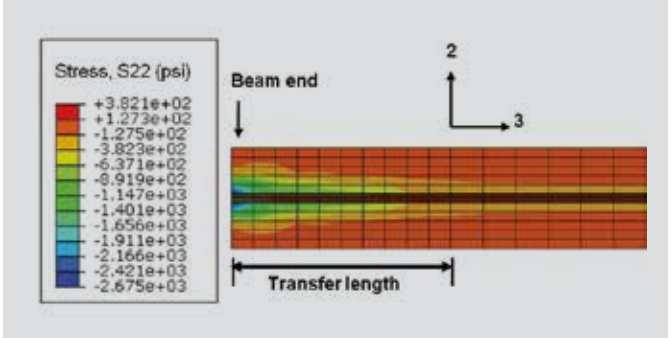

Figure 6. Contours of stress component S22 along vertical midplane from C1.00.NG beam model. Note: NG = fully bonded strand with gradual strand release. 1 psi = 6.895 kPa.

Strand expansion and Hoyer's effect

When the prestressing strand is released, the part outside the concrete recovers its original diameter while expansion of the portion embedded in the concrete is constrained. This leads to a change in the strand diameter along a portion of its length from the beam end. This difference in diameter produces a wedging effect commonly called Hoyer's effect.

Hoyer's effect has long been considered an important mechanism contributing to the transfer of stress between strand and concrete. Yet, in spite of its history, its true nature and relevance are still questioned. The simulations in this study allowed the opportunity to explore Hoyer's effect and its role in stress transfer because the strands were simulated as 3-D parts.

Figure 6 shows a contour plot of the vertical transverse stresses (S22) along the midsection of beam C1.00.NG. The stresses in the concrete close to the strand are negative (in compression). This compressive stress is greatest at the end of the beam and decreases along the transfer region. This behavior follows from the fact that the strand part outside the beam is free to expand while the expansion is restrained by the surrounding concrete in the transfer region. Beyond the transfer region, the strand experiences minimal dilation due to elastic shortening and time-dependent effects. Strand dilation at the beam end leads to increased bond resistance due to the greater normal pressure between strand and concrete. This primarily affects the adhesion type bond resistance mechanism. A second mechanism of stress transfer results from the wedge-shaped geometry that develops as the strand dilation decreases over the transfer zone. **Figure 7** shows this effect in the stress contour plots, which highlight the effects of strand debonding material on longitudinal stress transfer, and is discussed in detail in the next section. The contour plot for beam

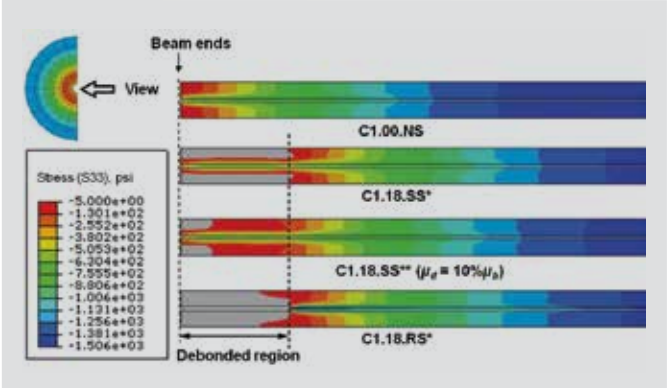

Figure 7. Contours of stress component S33 along vertical midplane from beam model C1.00.NS along with modified versions (shown by asterisks) of beams C1.18.SS and C1.18.RS. Modifications consisted of using the same coefficient of friction for all models (that of C1.00.NS) along the fully bonded region instead of the one obtained from model calibration. Note: NS = fully bonded with sudden strand release; RS = rigid sheathing with sudden strand release; SS = soft sheathing with sudden strand release; μ_b = friction coefficient between strand and concrete in finite element model along the bonded region; μ_d = friction coefficient between strand and concrete in finite element model along the debonded region. 1 psi = 6.895 kPa.

model C1.18.SS* (the asterisk indicates it is a modified version of C1.18.SS) shows the longitudinal stresses (S33) for a beam with an ideally debonded (friction coefficient between strand and concrete in finite element model along the debonded region μ_d equals 0) strand but with a tight-fitting geometry with the surrounding concrete. A nominal longitudinal stress is transferred within the debonded region. The stress transfer along this region is only due to the wedge effect created by the strand as it dilates and the resulting longitudinal reaction developed on the concrete part. Thus, the bond resistance mechanism behind Hoyer's effect follows from the friction resistance created by the larger strand/concrete contact pressure at the beam end and the longitudinal reaction provided by the hardened concrete against the diameter-varying strand (geometric wedge anchorage). While the contribution of Hoyer's effect to stress transfer relative to other mechanisms could not be fully assessed with the strand modeled as a rod, a simple assessment of the results suggests that its contribution is considerably smaller than that offered by the mechanical interlock resistance provided by the helical pattern of the strand.

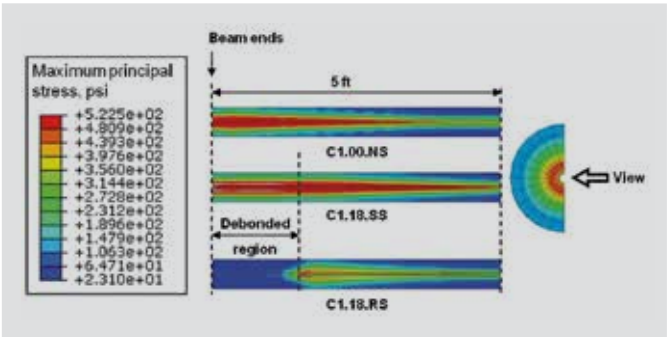

Figure 8. Maximum principal stresses in vertical midplane for C1 beam models. Note: NS = fully bonded with sudden strand release; RS = rigid sheathing with sudden strand release; SS = soft sheathing with sudden strand release. 1 ft = 0.305 m; 1 psi = 6.895 kPa.

Effect of debonding material

The models for the C1 beam series (6 in. [150 mm] diameter circular beams with a single concentric strand) were used to assess the effects of the debonding material, beginning with its effect on the transmission of longitudinal stresses. Figure 7 shows contour plots for the longitudinal stresses (S33) in the vertical midplane of beam C1.00.NS along with modified versions (identified with asterisks) of beams C1.18.SS and C1.18.RS. The modifications consisted of adopting the same coefficient of friction along the bonded region for all models (that of C1.00.NS, or μ_b equal to 0.23) instead of the one obtained from model calibration (Table 3). The results for beam C1.00.NS show the gradual transmission of axial compressive stresses along the beam length. When the strand is debonded with an oversized rigid sheathing (C1.18.RS*), the stress transfer distribution is simply shifted by the unbonded length with no longitudinal stress transfer along the debonded region.

Conversely, the results for C1.18.SS* show that longitudinal stresses actually get transferred along the debonded region if the strand is modeled as debonded with a tight-fitting shielding material that provides perfect debonding (μ_d equals 0). The mechanism of bond transfer is from the wedging component of Hoyer's effect as discussed. Because a flexible, tight-fitting debonding material may not fully eliminate all of the bond resistance (adhesion and mechanical interlock), case C1.18.SS** is presented, in which the coefficient of friction along the debonded region μ_d is taken as 10% of the friction coefficient in the bonded region (μ_b equal to 0.23). This nominal increase in bond resistance leads to a higher transmission of longitudinal stresses along the debonded region.

This effect was also quantified with the simulated data by extracting the strand slip into the beam after release. The ratio of the strand end slips for models C1.18.SS*, C1.18.SS**, and C1.18.RS* with respect to that of beam C1.00.NS were 1.74, 1.65, and 1.77, respectively. The ratios indicate that the strand pulls into the beam more than the fully bonded case due to the increased free strand length from the unbonded region. However, strand pull-in decreases if tight-fitting debonding is provided, even for the case of perfect debonding, and the presence of nominal bond resistance along the debonded region leads to a measurable transfer of longitudinal stresses along the debonded length. The presented results and discussions are supported by experimental data in the studies by Pavelchak[5] and Sun.[13]

The second effect of interest is that of strand dilation on the concrete element as a result of the debonding material. **Figure 8** shows contours of the maximum principal stresses in the vertical midplane of the C1 beams, and **Fig. 9** shows a plot of the principal tensile stress along a path on top of the beams. A region of high tensile stresses is generated close to the strand (Fig. 8). For beam C1.00.NS,

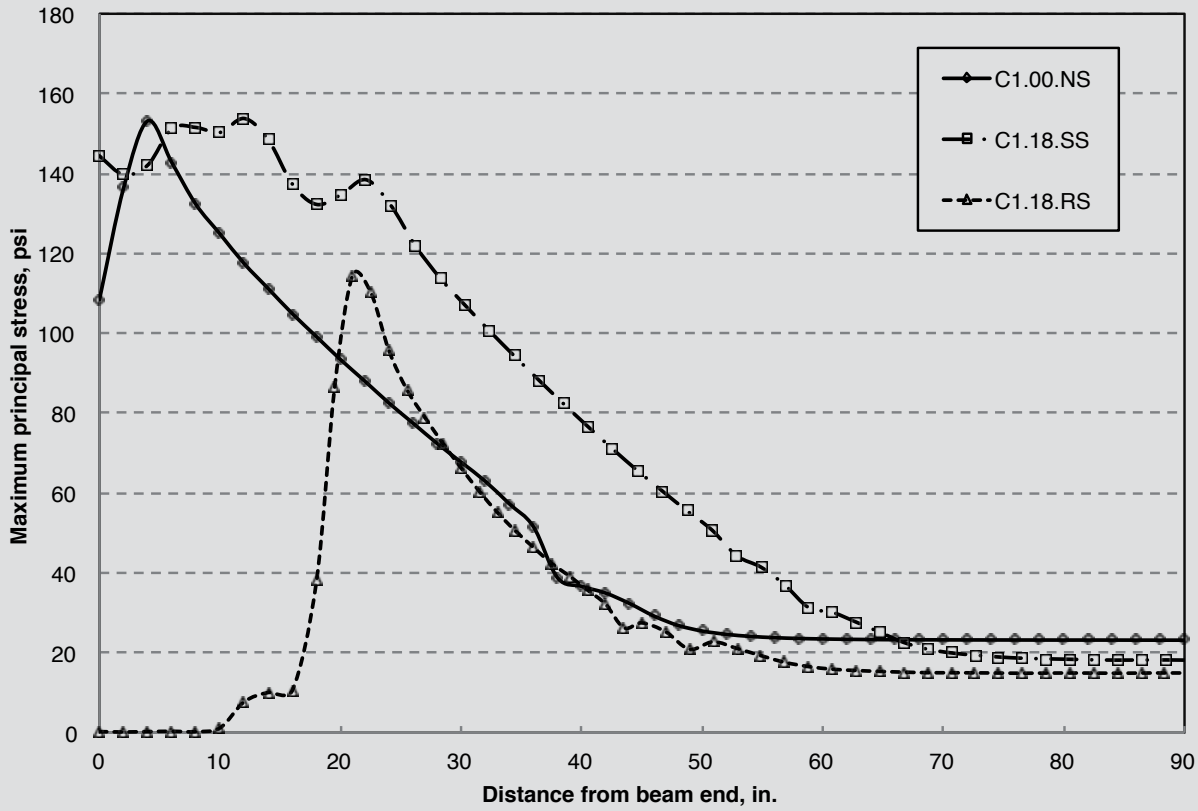

Figure 9. Comparison of maximum principal stresses (psi) along top surfaces for the C1 beam models. Note: NS = fully bonded with sudden strand release; RS = rigid sheathing with sudden strand release; SS = soft sheathing with sudden strand release. 1 in. = 25.4 mm; 1 psi = 6.895 kPa.

high tensile stresses concentrate in a region close to the beam end and decrease rapidly along the beam length (Fig. 9). For beam C1.18.RS, in which the strand is ideally debonded (rigid oversized sheathing), the principal tensile stresses in the debonded area are essentially eliminated while the stress beyond the debonded region is also reduced. Conversely, Fig. 8 and 9 show that the C1.18.SS model predicts the generation of high tensile stresses all along the debonded region and that their decay beyond the debonded length is similar to the end region of the fully bonded beam unit. These results show that debonding with a soft, tight-fitting sheathing material delays the decrease of principal tensile stresses and high stress values are sustained throughout the debonded region.

Effect of debonded length

The effect of debonded length was studied using models for the R2 beam series. **Figures 10** and **11** show contour plots and traces of maximum principal stresses for beams R2.00.NS, R2.18.SS, R2.36.SS, and R2.60.SS. Figure 10 shows that the high tensile stress region around the strands tends to grow toward the top and bottom surfaces of the beams (**Fig. 12** also shows this with a contour of maximum principal strains). This is different from the distribution of high tensile stresses for the beams with one strand, in which the high stress region was uniformly distributed around the strand. This change in response is attributed to the reduced concrete cover above and below the strands (Fig. 2). Figure 10 also shows that the tensile stresses near the top and bottom surfaces remain high throughout the entire debonded length.

Figure 11 shows traces of the principal tensile stress along a path centered on the beam top surface. For the beams with debonded

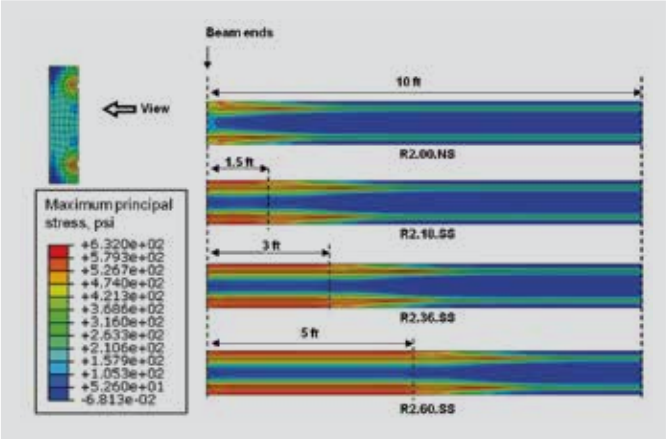

Figure 10. Maximum principal stresses on vertical midplane for R2 beam models. Note: NS = fully bonded with sudden strand release; SS = soft sheathing with sudden strand release. 1 ft = 0.305 m; 1 psi = 6.895 kPa.

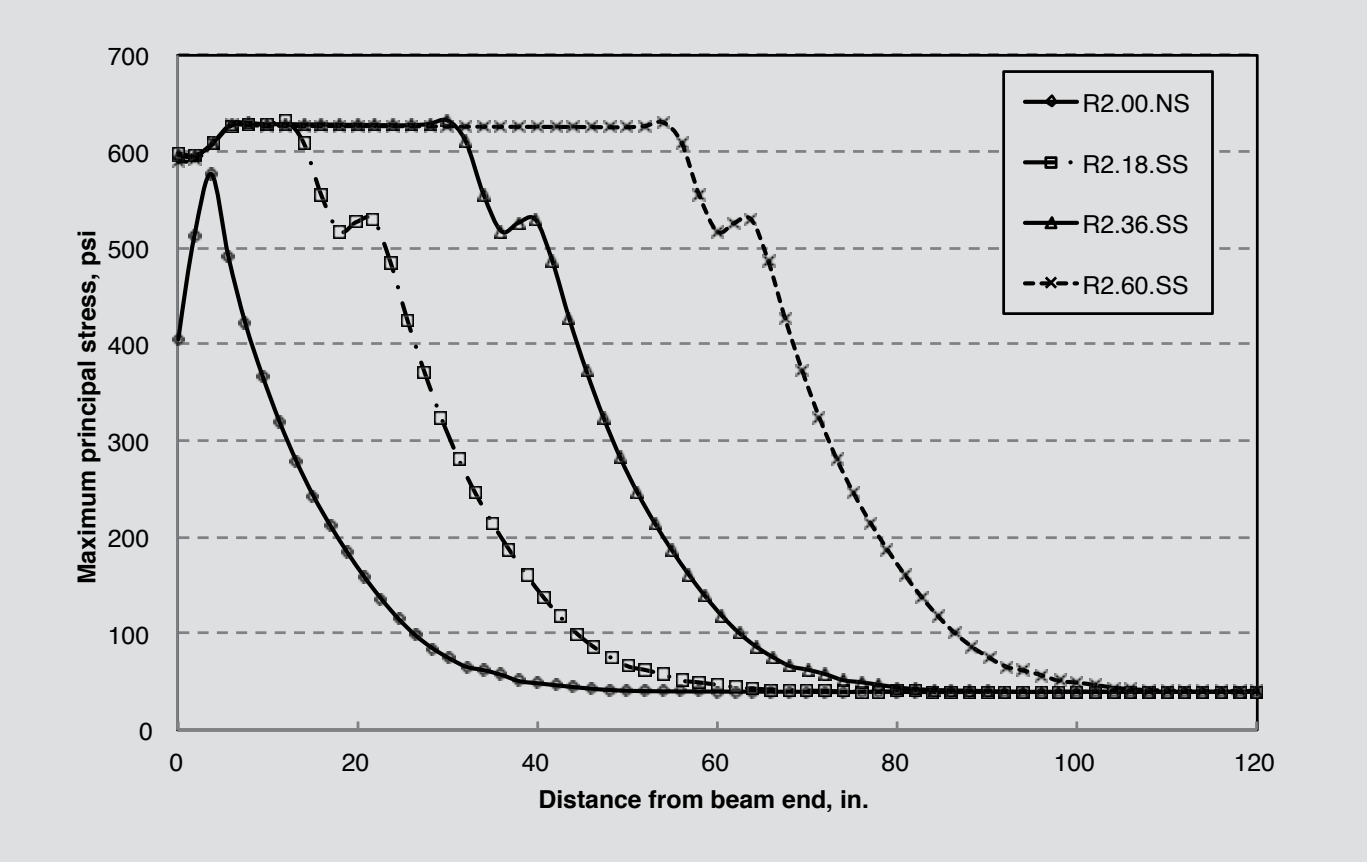

Figure 11. Maximum principal stresses along top surface path of R2 beam models. Note: NS = fully bonded with sudden strand release; SS = soft sheathing with sudden strand release. 1 in. = 25.4 mm; 1 psi = 6.895 kPa.

strands the tensile stresses along the debonded length are higher than the maximum stress in the fully bonded beam (R2.00.NS). Further, the results show that strand debonding delays the decrease of the tensile stress. Figure 12 shows contours of the principal tensile strains at the end section of beams R2.00.NS and R2.18.SS. In the debonded case the strain around the strand is greater and thus more likely to produce longitudinal splitting cracks at the top and bottom surfaces of the beam.

Effect of adjacent strands

Figures 13, **14**, and **15** present results for the beam models with four strands (R4 cross section). Figure 13 shows contours of the equivalent plastic strains (a scalar indicator of accumulated plastic damage) on the end cross section of the R4 beams. Plastic strains developed around the strands for all beam units except for beam R4.36.RS, which is the beam with rigid oversized debonding material. The plastic strain regions around the strands in other beams grew radially but did not merge. However, it can be expected that if the concrete tensile strength is lower, the two plastic regions may join, which would imply cracking between the strands. Figure 13 shows evidence to this effect. The contours of the principal tensile strains reveal that the strains in the region between the adjacent strands were high. Further, a small high-strain region on the top and bottom surfaces was also apparent for beams R4.36.SS and R4.60.SS, which indicates that cracking may propagate to these surfaces.

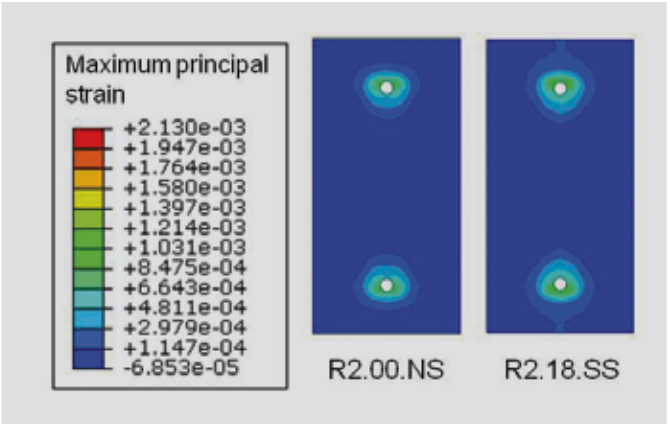

Figure 12. Maximum principal (tensile) strain contours for R2.00.NS and R2.18.SS beam models at their end section. Note: NS = fully bonded with sudden strand release; SS = soft sheathing with sudden strand release.

The high tensile stress region in the first three beams was generally close to the strands (Fig. 13). High stresses were predicted at the top and bottom surfaces for beams R4.36.SS and R4.60.SS, and the stresses between the top and bottom strand pairs in these two models were lower. This is due to the lower concrete strength of these two beams compared with the other R4 beams (Table 1) and because the concrete in the highly stressed regions lost stiffness due to damage. The growth of the high tensile stress region can be separated into two forms:

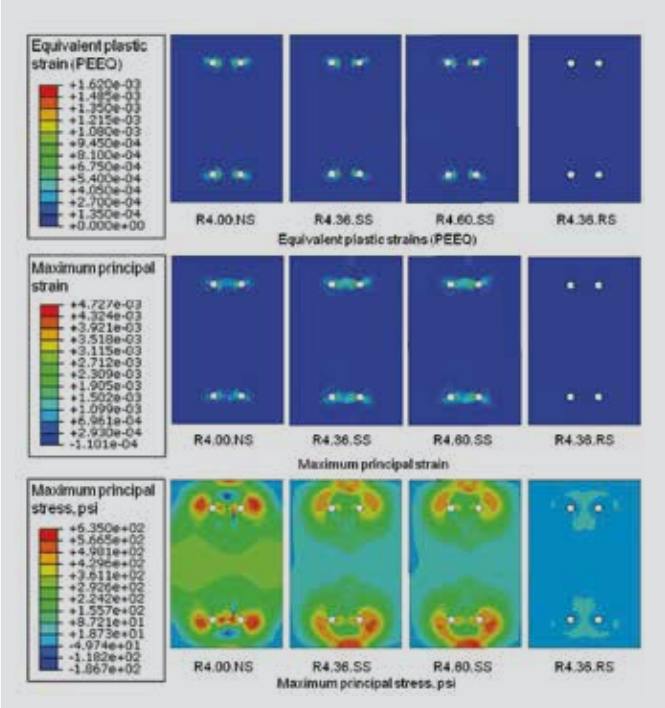

Figure 13. Strain and stress contours at end cross sections of R4 beam models. Note: NS = fully bonded with sudden strand release; RS = rigid sheathing with sudden strand release; SS = soft sheathing with sudden strand release. 1 psi = 6.895 kPa.

- high tensile stresses between adjacent strands that propagate horizontally and merge
- high tensile stresses that propagate toward the nearest free edge at an angle of approximately 45 degrees and create high-stress regions on the beam surface

Figure 14 shows contour plots of the principal tensile stresses along the top surfaces of the R4 beams. The high-stress regions were caused by the vertical propagation of high tensile stresses from the top strands (Fig. 13). For the fully bonded beam, the high-stress region only developed near the beam end. For beam R4.36.RS, the high-stress region shifted from the beam end to the onset of bond due to the ideal debonding provided by the rigid oversized sheathing. For this same beam, the stresses observed within the debonded region were caused by the localized effect at the onset of full strand bond inside the beam, but their magnitude was much smaller. Conversely, for beams R4.36.SS and R4.60.SS the region with high tensile stresses was not only present at the onset of full strand bond condition but also along the full debonded length. As explained before, this behavior is due to the radial expansion of the debonded strand and the pressure that it exerts on the concrete by virtue of the tight fit between the strand and concrete.

Figure 15 shows traces of the principal tensile stresses for the R4 beams along the centerline of their top surface. The traces show that the tensile stress distribution for beams R4.00.NS and R4.36.RS reached a peak value a few inches after the start of the full bond condition and decreased rapidly after that. Further, the tensile stress in the debonded region for beam R4.36.RS was essentially zero. For beams R4.36.SS and R4.60.SS, the maximum tensile stresses also occurred a few inches after the full bond condition starts and decayed rapidly as well. However, the principal tensile stresses for these beams along the debonded length of the strand were significant. Further, unlike the R2 beam models, the stress in the debonded region was less than the peak stresses. This is because the concrete along the debonded region in the R4.36.SS and R4.60.SS beam models suffered damage, as evidenced in Fig. 13 by the high-strain region at the top of the beams.

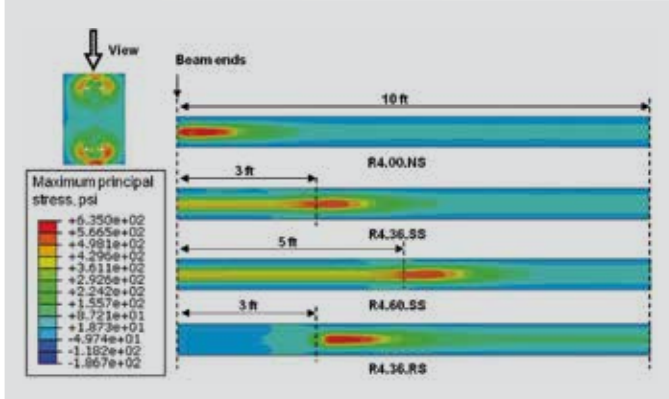

Figure 14. Maximum principal stresses on top surface of R4 beam models. Note: NS = fully bonded with sudden strand release; RS = rigid sheathing with sudden strand release; SS = soft sheathing with sudden strand release. 1 ft = 0.305 m; 1 psi = 6.895 kPa.

Discussion

Based on the results and discussion from the previous sections, it follows that the concrete around a shielded prestressing strand will be highly stressed within the debonded region if the strand and concrete have tight contact. The reason follows from the fact that the absence of bond strength will maximize expansion of the strand after release. This phenomenon is explained in the following paragraphs with reference to the equivalent system in **Fig. 16**.

Consider a small strand segment in which the expansion of the strand after pretension release is represented by an equivalent longitudinal (that is, axial) compressive force ΔF. The force ΔF can be considered to be the force drop in the small strand segment along the transfer region after release. The bond strength between strand and concrete is represented by two springs in the longitudinal direction with longitudinal stiffness K_L, and the radial interaction (or normal interaction between strand and concrete surfaces) is represented by two springs in the transverse direction with stiffness K_T.

By considering equilibrium for the system and loading in Fig. 16, if the longitudinal stiffness K_L is high (bond strength is high) the axial force ΔF will be balanced by the force in the two longitudinal springs with small longitudinal deformation Δ_L. Thus, the transverse deformation Δ_T,

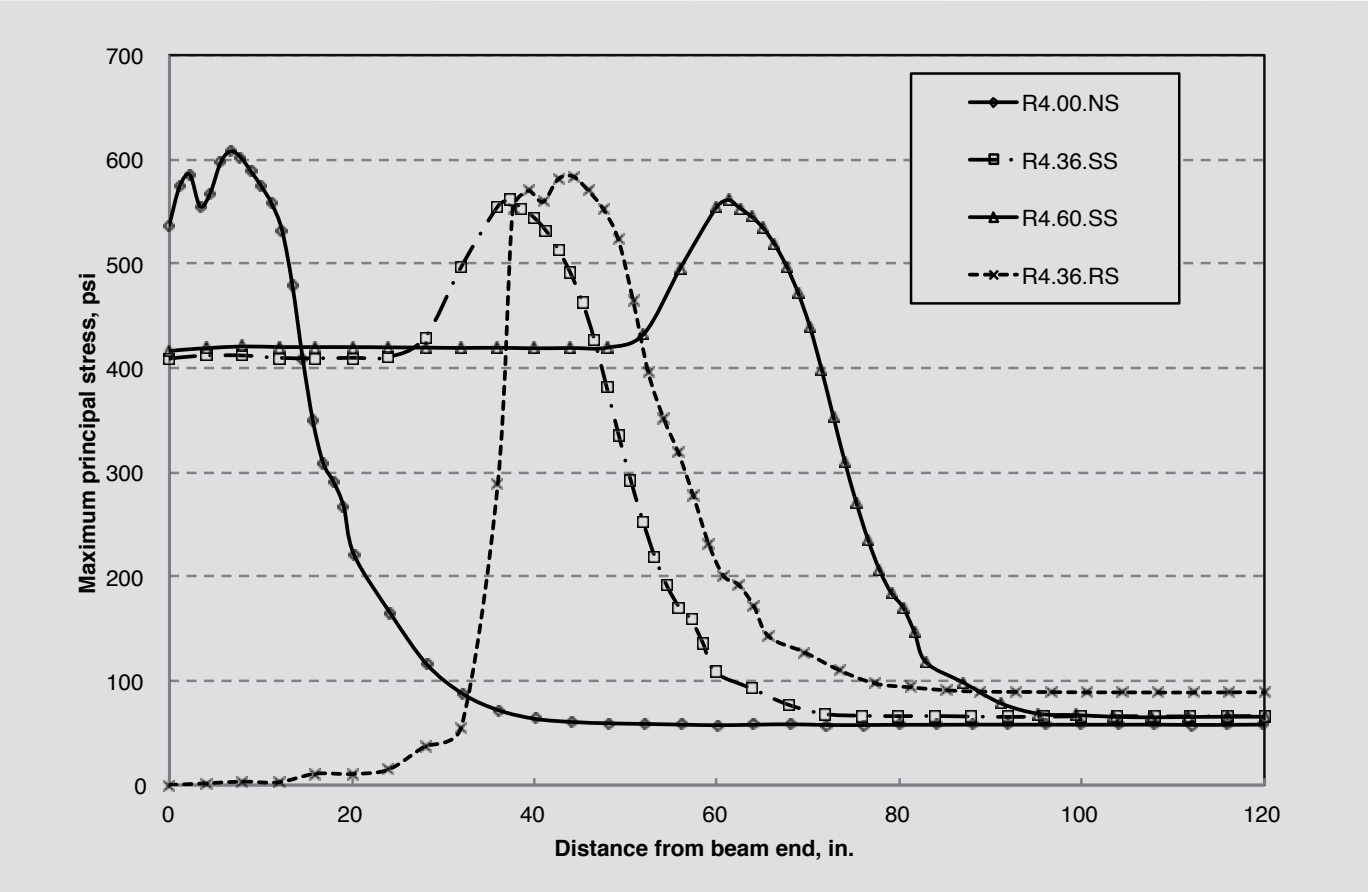

Figure 15. Maximum principal stresses along top surface path of R4 beam models. Note: NS = fully bonded with sudden strand release; RS = rigid sheathing with sudden strand release; SS = soft sheathing with sudden strand release. 1 in. = 25.4 mm; 1 psi = 6.895 kPa.

which is related to Δ_L by the Poisson's ratio of the strand, is small. As a consequence, the force in the transverse springs F_T (equal to $\Delta_T K_T$) will also be small.

On the other hand, if the longitudinal springs have low stiffness (poor bond strength), the equivalent axial compressive force ΔF will not be balanced until a relatively large longitudinal deformation takes place. Consequently, the transverse strand deformation will be greater and so will the force in the transverse springs. It follows that if the longitudinal stiffness K_L is zero (if it has no bond strength at all) the equivalent axial compressive force ΔF will be completely balanced (actually dissipated) by the longitudinal strand deformation and its transverse expansion will be maximized. This is the reason why the finite element simulations have shown that concrete within the debonded region will be highly stressed if there is no room for the strand to expand freely. Such a phenomenon also implies that the radial expansion of strand after its release will be increased if the strand has substandard bond quality. Finally, the effect of confinement reinforcement for controlling the dilation-induced cracking by soft sheathing debonding was not part of this study, but Donoso[18] studied this effect using similar numerical methods and found the beneficial effect to be minimal.

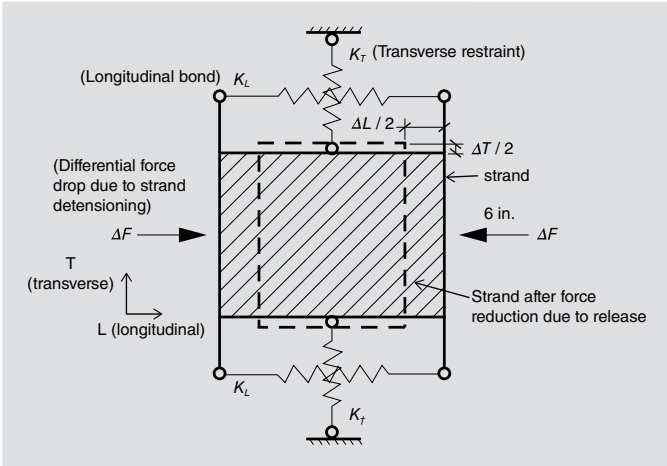

Figure 16. Free body diagram of small strand segment under effect of differential force change during stress transfer. Note: K_T = stiffness of spring in the transverse (radial) direction; K_L = stiffness of spring in the longitudinal (axial) direction; Δ_T = deformation of spring in the transverse (radial) direction; Δ_L = deformation of spring in the longitudinal (axial) direction; ΔF = equivalent axial compressive force.

Conclusion

The following conclusions are offered based on the presented computational study of the stress-transfer characteristics in fully bonded and partially debonded prestressed concrete beams:

- Debonded strands with flexible tight-fitting sheathing

can lead to additional stresses in the concrete along the entire debonded length due to the increased radial expansion that occurs as a consequence of the reduced bond strength. The numerical simulations indicated that if the concrete and strand have tight contact and the coefficient of friction between the strand and the concrete is reduced (or worse, eliminated), the internal pressure on the concrete surrounding the strand is high due to the strand's radial expansion. Thus, concrete in the debonded region will be stressed and the magnitude of the stress will be maintained constant throughout the debonded region, only to decrease after the full bond condition starts. The additional stresses can lead to concrete cracking by themselves or when combined with stresses caused by production (detensioning), dead loads, or service demands.

- The use of oversized rigid sheathing can avoid damage from the dilation of debonded strand. If the strand is ideally debonded and there is enough room around the strand for it to dilate freely, the stress in the debonded region can be significantly reduced.

- Concrete damage due to the dilation of debonded strand with tight-fitting flexible sheathing can be more severe for adjacent debonded strands as the tensile stress states overlap. The simulations showed that the high tensile stress regions around adjacent strands tend to propagate and merge with each other. In addition, based on the observed distribution of principal tensile stresses, cracks also tend to propagate toward the closest free surface.

- The behavior of debonded strands with tight flexible sheathing is analogous to that of a strand with poor bond quality. Thus, strand with poor bond quality will generate similarly high tensile stresses that can lead to cracking in the concrete element, a condition that is well recognized.

The following recommendations are offered for design and construction practice:

- Strand debonding with flexible sheathing or any type of debonding method that leads to a tight fit between the strand and concrete (for example, duct tape) with a low coefficient of friction between the sheathing and the strand is not recommended because it can lead to concrete cracking due to the additional stresses that are developed with this detail.

- The use of oversized sheathing for strand debonding is recommended for minimizing adverse effects of cracking, particularly in congested sections or those with end skew geometry. The oversized sheathing should have an inside diameter that exceeds the nominal diameter and allows for warping and wobbling. Based on this study and the accompanying experimental work,[4] closed tubing with an inner diameter larger than the nominal strand diameter by $^1/_8$ in. (3.2 mm) is recommended. The oversized sheathing should be rigid enough so that it does not collapse (in other words, squeeze and create a tight fit with the strand) under the weight of the fresh concrete during construction. The ends of the sheathing material should be sealed with tape.

- The debonding of adjacent strands (both horizontally and vertically) and exterior strands that are closest to the concrete surface is not recommended when flexible or tight-fitting sheathing is used.

Acknowledgments

The material presented in this paper was part of a research project funded by the Michigan Department of Transportation (MDOT). The authors sincerely appreciate the help received from Mr. Tom Grumbine, formerly at the Premarc Corporation (Grand Rapids, Mich.), through his support of the associated experimental study and the valuable information and insight that he shared on the production of prestressed concrete bridge beams.

Disclaimer

The opinions, findings, conclusions, and recommendations presented in this paper are those of the authors alone and do not necessarily represent the views and opinions of Michigan State University or the Michigan Department of Transportation.

References

1. ACI Committee 318. 2011. *Building Code Requirements for Structural Concrete (ACI 318-11) and Commentary (ACI 318R-11)*. Farmington Hills, MI: ACI.

2. AASHTO (American Association of State and Highway Transportation Officials). 2012. *AASHTO LRFD Bridge Design Specifications*. 6th ed. Washington, DC: AASHTO.

3. Grumbine, T. 2004. Premarc/Marsh Products Inc., Personal communication.

4. Burgueño, R., and Y. Sun. 2011. "Effect of Strand Debonding on the Production and Performance of Prestressed Concrete Beams." Research report RC-1546. Report to the Michigan Department of Transportation, Department of Civil and Environmental Engineering, Michigan State University, East Lansing, MI.

5. Pavelchak, M. A. 2009. "Factors for Improving the Design and Construction of U-Beam Bridges: Live

Load Distribution and Prestressing Strand Debonding Effectiveness." MS thesis. Department of Civil and Environmental Engineering, Purdue University, West Lafayette, IN.

6. Mirza, J. F., and M. E. Tawfik. 1978. "End Cracking in Prestressed Members during Detensioning." *Modern Concrete* 42 (2): 44–49.

7. Ghosh, S. K., and M. Fintel. 1986. "Development Length of Prestressing Strands, Including Debonded Strands, and Allowable Concrete Stresses in Pretensioned Members." *PCI Journal* 31 (5): 38–57.

8. Kannel, J., C. French, and H. Stolarski. 1997. "Release Methodology of Strands to Reduce End Cracking in Pre-tensioned Concrete Girders." *PCI Journal* 42 (1): 42–54.

9. Oh, B. H., E. S. Kim, and Y. C. Choi. 2006. "Theoretical Analysis of Transfer Lengths in Pretensioned Prestressed Concrete Members." *Journal of Engineering Mechanics* 132 (10): 1057–1066.

10. Okumus, P., and M. P. Oliva. 2013. "Evaluation of Crack Control Methods for End Zone Cracking in Prestressed Concrete Bridge Girders." *PCI Journal* 58 (2): 91–105.

11. Janney, J. 1954. "Nature of Bond in Pre-tensioned Prestressed Concrete." *ACI Journal* 25 (9): 717–736.

12. De Nardin, S., F. M. Almeida Filho, J. Oliveira Filho, V. G. Haach, and A. L. H. C. El Debs. 2005. "Nonlinear Analysis of the Bond Strength Behavior on the Steel-Concrete Interface by Numerical Models and Pull-out Tests." In *Proceedings of the 2005 Structures Congress and Exposition*. New York, NY: American Society of Civil Engineers (ASCE).

13. Sun, Y. 2010. "Effect of Strand Debonding on End Cracking in Pre-tensioned Concrete Beams." MS thesis. Department of Civil and Environmental Engineering, Michigan State University, East Lansing, MI.

14. Lee, J., and G. L. Fenves. 1998. "Plastic-Damage Concrete Model for Cyclic Loading of Concrete Structures." *Journal of Engineering Mechanics* 124 (8): 892–900.

15. Collins, M. P., D. Mitchell, and J. G. MacGregor. 1993. "Structural Design Considerations for High-Strength Concrete." *Concrete International* 15 (5): 27–34.

16. ACI Committee 318. 2008. *Building Code Requirements for Structural Concrete (ACI 318-08) and Commentary (ACI 318R-08).* Farmington Hills, MI: ACI.

17. Russell, B. W., and N. H. Burns. 1993. "Design Guidelines for Transfer, Development and Debonding of Large Diameter Seven Wire Strands in Pretensioned Concrete Girders." Research report 1210-5F. Center of Transportation Research, Bureau of Engineering Research, University of Texas at Austin.

18. Donoso, M. 2011. "Effect of Partial Debonding of Prestressing Strands on Beam End Cracking." MS thesis. Department of Civil and Environmental Engineering, Michigan State University, East Lansing, MI.

Notation

E_c = elastic modulus of concrete at day of test

E_p = elastic modulus of prestressing strand at day of test

f'_{ci} = concrete compressive strength at time of initial prestressing

F_T = force in spring in transverse (radial) direction

K = ratio of second stress invariant on tensile meridian to that on compressive meridian at initial yield for any given value of pressure invariant such that maximum principal stress is negative

K_L = stiffness of spring in longitudinal (axial) direction

K_T = stiffness of spring in transverse (radial) direction

L = beam length

L_b = bonded region length

$L_{t,Exp}$ = transfer length from experimental data

$L_{t,FE}$ = transfer length from finite element data

L_u = unbonded region length

Δ_T = deformation of spring in transverse (radial) direction

Δ_L = deformation of spring in longitudinal (axial) direction

ΔF = equivalent axial compressive force

μ_b = friction coefficient between strand and concrete in finite element model along bonded region

μ_d = friction coefficient between strand and concrete in finite element model along debonded region

σ_{b0} = initial equibiaxial compressive yield stress

σ_{c0} = initial uniaxial compressive yield stress

About the authors

Rigoberto Burgueño, PhD, is an associate professor of structural engineering in the Department of Civil and Environmental Engineering at Michigan State University in East Lansing, Mich.

Yi Sun is a PhD student and graduate research assistant in the Department of Civil and Environmental Engineering at Michigan State University.

Abstract

Strand debonding is a common approach used to control stress and reduce cracking at the ends of pretensioned concrete beams. However, damage in pretensioned beams with debonded strands during manufacture has raised concerns about the use of debonding as currently specified. Numerical simulations were conducted in this study to improve understanding of the stress transfer characteristics of sheathed strand in pretensioned concrete elements. Nonlinear finite element models of small-scale prestressed concrete beam units in which concrete and strand were modeled with three-dimensional continuous elements were established with commercial software. The numerical simulations were calibrated with experimental data, and results show that the lack of bond resistance along the debonded region maximizes the dilation of the strand after release. This effect may damage the concrete if there is tight contact between concrete and strand, which may result when using flexible, tight-fitting debonding material. This problem is eliminated if enough room is provided for strand dilation.

Keywords

Debonding; finite element method; sheathing; simulation; strand; stress transfer; transfer length.

Review policy

This paper was reviewed in accordance with the Precast/Prestressed Concrete Institute's peer-review process.

Reader comments

Please address and reader comments to journal@pci.org or Precast/Prestressed Concrete Institute, c/o *PCI Journal*, 200 W. Adams St., Suite 2100, Chicago, IL 60606.